Growth and overgrowth of concentrated gold nanorods: Time resolved SAXS and XANES

ARTICLE *in* CRYSTAL GROWTH & DESIGN · MARCH 2012

Impact Factor: 4.89 · DOI: 10.1021/cg2016116

CRYSTAL GROWTH & DESIGN

Article

pubs.acs.org/crystal

Growth and Overgrowth of Concentrated Gold Nanorods: Time Resolved SAXS and XANES

F. Hubert,[†] F. Testard,[†] A. Thill,[†] Q. Kong,[‡] O. Tache,[†] and O. Spalla*[,†]

[†]CEA Saclay, DSM/IRAMIS/UMR 3299 CEA/CNRS SIS2M/Laboratoire Interdisciplinaire sur l'Organisation Nanométrique et Supramoléculaire, 91191 Gif sur Yvette, France

[‡]Synchrotron SOLEIL, L'Orme des Merisiers Saint-Aubin, BP 48 91192 Gif sur Yvette Cedex, France

Supporting Information

ABSTRACT: The growth of gold nanorods has been followed by small angle X-ray scattering and X-ray absorption. The synthesis is performed at high concentration of 3.5 mM in gold using in situ generation of seeds. It is shown that the growth occurs at constant number density of nanoparticles after the initial nucleation of seeds and that the final step of reduction of Au(I) to Au(0) occurs only at the surface of the growing nanorods. Anisotropy is acquired during the growth with a ratio of longitudinal to basal growth rates measured at 12. The final aspect ratio is only limited by the available amount of material and the experiment of overgrowth was allowed to reach a final aspect ratio of 5 instead of the initial 3.6.

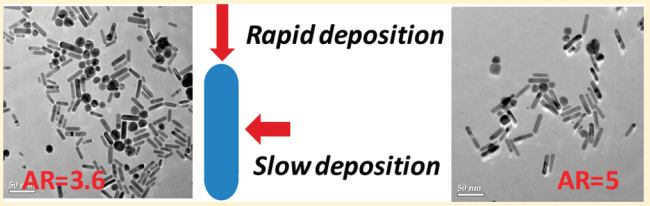

INTRODUCTION

Among the metal nanoparticles that are synthesized nowadays, gold nanorods GNRs have raised great hopes for many biological and medical applications.[1,2] These particles exhibit transverse and longitudinal surface plasmon bands sensitive to the local chemical environment. As the absorption wavelengths are also related to their aspect ratio (AR), its control appears of primordial importance.[3] Many schemes of synthesis are now available and among them the wet route starting from dilute solution of gold(III) ions is effective to produce a large volume of dilute suspension with a rather fine empirical control of the AR through a suitable choice of chemical conditions (amount and type of surfactant, addition or not of silver nitrate, temperature, concentration of seeds, amount of reducing agent).[4−7] Most of the synthesis are performed at low concentration (around 0.5 mM in gold) in order to diminish the pollution by different other shapes such as spheres and triangles. Moreover, even in the most popular seeded growth method with excess CTAB (cetyltrimethylammonium bromide), a purifying step remains mandatory. Hence, from a practical point of view, challenges for physical chemists are still to obtain GNRs in a concentrated amount without further separation processes.[8] These experimental difficulties are related to an incomplete understanding of the mechanisms ruling the final size, AR, polydispersity, and even surface structure of the GNRs.[9−11]

One major open question regards the time scale at which anisotropy develops and the underlying microscopic mechanism of shape selection.[12] One route contributing to unravel mechanisms consists of measuring the kinetics of important characteristics during the formation of the particles.[13] In the last five years, time-resolved experiments were performed using different methods such as UV, small-angle X-ray scattering (SAXS), wide-angle X-ray scattering (WAXS), and X-ray absorption fine structure (XAFS). Although not an in situ experimental technique, transmission electron microscopy (TEM) has also been used to obtained low time resolution by freezing the system at different stages of development.

Using UV experiments, Bullen et al.[14] systematically investigated the kinetics of silver mediated seeded growth GNRs. They extracted the initial growth rate for different chemical conditions and showed that the depletion of gold ions has a linear dependence on gold salt concentration and seed concentration. The influence of the pH on the growth rate was attributed to the concentration of the reducing ascorbate monoanions. Regarding morphology, UV−visible spectroscopy also offers the following of the AR from the longitudinal surface plasmon band.[3,15−17] The higher the AR, the higher the plasmon peak wavelength. However, UV spectroscopy does not allow a separate measure of the width and the length of the GNRs, the yield of the reaction, and a quantification of the rod percentage among the different shapes. Accordingly, TEM was used to reveal the morphological changes during the nanoparticles formation.[18−21] One strong result is the large increase of the length as compared to the width dimension and it serves as a first base for development of models for anisotropic growth. TEM is generally used in support of other methods because of possible artifacts due to the drying step and time-consuming step to obtain statistical analysis on a large number of particles.

With the development of third generation synchrotron facilities, time-resolved SAXS is becoming a technique of choice to follow the formation of nanoparticles with a quantitative measure of the different dimensions and the total concentration in

Received: December 6, 2011
Revised: January 6, 2012
Published: January 27, 2012

   dx.doi.org/10.1021/cg2016116 | *Cryst. Growth Des.* 2012, 12, 1548−1555

nanoparticles. The analysis is obtained on a large volume ensuring a measure of the averages of the morphological characteristics. Widely used for isotropic nanoparticles, few studies concern the GNRs. Recent works however addressed the seeded growth method at low concentration.[22,23] Henkel et al.[22] have obtained the time variation of the length and width of GNRs during their formation. Using a Gaussian distribution for L and D they reported a maximum in the AR versus time also observed by UV. This maximum results from different decay times for length growth rate and diameter growth rate and was attributed to a depletion of reactants as ascorbic acid concentration was only 1.1 higher than the gold concentration (under stoichiometric conditions). The proposed mechanism is a shift from a one-dimensional (1D) growth to a three-dimensional (3D) growth, resulting in a smaller final AR than the one expected from the initial growth rates (the longitudinal growth rate being five time higher than the transverse one). Morita et al.[23] used time-resolved distance distribution functions for similar synthetic conditions. They found the crossover of growth rates after 8−12 min in agreement with Henkel et al.[22] for an AR of 2 or 4, but not for an AR of 6. The ratio of the length growth rate to the diameter growth rate was found to depend strongly on the final AR controlled by the amount of silver nitrate in the solution (4.5 for AR2 and 8 for AR4).

In this work, we investigate the GNRs formation using combined time-resolved SAXS and X-ray absorption near edge structure (XANES) for concentrated gold solution using an in situ seed generation method. The gold concentration used for this study is 3.5 mM (six times higher than the classical studies of the literature) leading to more concentrated GNRs solution in the aqueous phase. We used the quantitative approach described in our recent paper on gold nanosphere synthesized in organic solvent[24] to investigate the kinetic of GNRs formation, coupling SAXS, and XAS experiments. While SAXS is sensitive to the growing nanoparticles, XANES is sensitive to the concentration of the different redox states of gold.[25] Using absolute scaling units for SAXS experiments and the non-Gaussian (L, R) distribution recently evidenced by TEM,[26] we are able to obtain the number density of objects with time, their dimensions, and polydispersity. In parallel, dispersive XANES allows us to obtain a good statistic at the time scale of the experiment for the gold speciation during the GNRs formation. The obtained combined information gives a unique set of data to go deeper into the mechanism.

MATERIALS AND METHODS

Synthesis Scheme. The GNRs were produced in aqueous solution using a seedless method adapted from the initial work of Jana.[6,27] A two stage method was used for the synthesis. First, an initial solution was prepared with four components; two of them were fixed for all the samples, i.e., 3.5 mM in $HAuCl_4$ and 0.2 M in CTAB. To 10 mL of this two component solution at 27 °C, a small volume of a 120 mM $AgNO_3$ solution was added to reach a final concentration going from 0 to 2 mM (160 μL). A 100 mM ascorbic acid solution was then added to reach a final concentration in the range 0−9.67 mM (960 μL) and was left to equilibrate for 1 min. The initially red solution ($HAuCl_4$, CTAB) became uncolored after the addition of ascorbic acid. In the second stage, a tiny volume (from 4 to 192 μL) of a ice-cooled borohydride solution at 1.6 mM was added to trigger the formation of seeds and the growth of the nanorods. In order to ensure the reproducibility of the synthesis scheme, a special attention was taken in the preparation and use of the borohydride. First, the borohydride solution was prepared in a 100 mL flask previously kept in an ice bath using water also kept in ice bath. The solution kept in an ice bath was used rapidly after the preparation. Second, the small volume was injected using a remotely controlled syringe pump with an accuracy below 1 μL. The synthesis as seen by TEM, SAXS, and XANES was fully reproducible in these experimental conditions. The conditions for the so-called reference synthesis correspond to the following final concentration of each component in the final solution: $HAuCl_4$ (3.5 mM), CTAB (0.2 M), $AgNO_3$ (1 mM), AA (4.8 mM), $NaBH_4$ (0.01 mM).

Regrowth synthesis conditions were as such: at the end of a given synthesis, the solution was left for 24 h before operating a regrowth experiment. Contrary to the classical regrowth experiment where only a small amount of seeds (or nanoparticles) is added in the growth solution, here the regrowth solution at the same gold concentration is added dropwise to the solution containing the nanorods to be overgrown. For the first regrowth, 10 mL of a growth solution ($HAuCl_4$ (3.5 mM), CTAB (0.2M), $AgNO_3$ (1 mM), ascorbic acid (4.8 mM)) is added to the initial 10 mL of nanorods solution. For the second regrowth, 10 mL of a growth solution ($HAuCl_4$ (3.5 mM), CTAB (0.2M), $AgNO_3$ (1 mM), ascorbic acid (4.8 mM)) is added to the 20 mL obtained after the first regrowth.

In Situ Small Angle X-ray Scattering and X-ray Absorption Spectroscopy. *Experimental Acquisition.* Two different types of experiments were combined in the present work. The SAXS experiment was performed at the ESRF (European Synchrotron Radiation Facility, Grenoble, France) on the high brilliance ID-2 beamline. The XANES at the L_{III} gold edge was recorded on the Dispersive EXAFS beamline (ODE) of the SOLEIL Synchrotron (Saint-Aubin, France). For the SAXS experiment the available q-range was 0.004−0.3A^{-1} using an incident beam energy of 11.5 keV below the L_{III} edge of gold. A two-dimensional (2D) scattering image was acquired within 100 ms. The scattering by the solution was isotropic and classical procedures of radial averaging and normalization were applied to obtain data at the absolute scale. In the case of XANES, the use of a dispersive setup allows a very high time resolution to be obtained. A curve Si(111) monocrystal disperses the X-ray beam on a CCD detector Princeton Instrument 7497-002 (2048 × 600 pixels de 7 μm). For each of the energy, the focal plane is the one of the camera. However, the different energies are spread on the whole detector. The camera was located 1 m after the sample. Comparing the intensity on the camera between an empty cell and a cell filled with the gold solution allows the transmission spectra to be obtained simultaneously in a large energy range (covering the gold edge). The total acquisition time for one spectrum was 800 ms of acquisition obtained by averaging 200 consecutive acquisitions of 4 ms each.

The nanoparticle synthesis was done in a controlled temperature double walled glassware of content 30 mL thermostatted at 27 °C. A peristaltic pump allowed circulation of the measuring solution which was coupled with UV detection. The cell for the SAXS experiment was a classical quartz capillary of 1.5 mm path length. For the XANES experiment, due to the very low concentration of gold (a few mM), a dedicated cell with a path of 10 mm was built to ensure a total jump of absorbance of 0.1 through the edge.[24] The first step solution containing ($HAuCl_4$, CTAB, $AgNO_3$, and ascorbic acid) is prepared in the thermostat cell and $NaBH_4$ was added in a few milliseconds using a remotely control motorized microsyringe. This injection defined the zero time of the experiment and was synchronized with the XANES or SAXS acquisition. The spectra (XANES) or scattering diagram (SAXS) was measured every 20 s during 30 min. Before each type of experiment (SAXS and XANES), the potential influence of the X-ray beam was controlled on a pure $HAuCl_4$ solution. In the case of XANES, the reduction down to Au(0) was less than 5% after 30 min of illumination (see Supporting Information Figure S1). Regarding SAXS, no particle formation was measurable.

XANES Treatment. Measuring the concentration of the gold species is mandatory to unravel the chemical pathways by which the nanorods appear. As the concentration of two of these species (Au(I) and Au(0)) cannot be measured by classical laboratory UV−visible spectroscopy, XANES was used to follow the concentration of all the gold species. Indeed, Au(III), Au(I), and Au(0) can be discriminated by XANES spectra at the L_{III} gold edge. The high concentration (3.5 mM) allowed accurate XANES signals to be obtained. They were obtained as follows: the Au(III) spectra comes from the initial $HAuCl_4$ solution.

dx.doi.org/10.1021/cg2016116 | Cryst. Growth Des. 2012, 12, 1548−1555

A signature of this oxidation state is a prepeak at around 11.920 keV. The Au(0) spectra was obtained from a gold foil. It features double peak, the first one (at 11.945 keV) being directly linked to the electronic state. Finally, a solution of Au(I) in a toluene/DDAB solution was obtained by a mild reduction with ascorbic acid of the initial Au(III) salt solution. We have verified that the obtained spectra is identical to a gold(I) salt powder (AuCl). The features of the Au(I) spectra are less marked since only a slight shoulder is seen at 11.925 keV. However, the lack of a peak at 11.920 and 11.945 keV allows separation of it from Au(III) and Au(0).

SAXS Treatment. During the synthesis, the signal from CTAB micelles is present due to the large concentration of CTAB. Figure 1

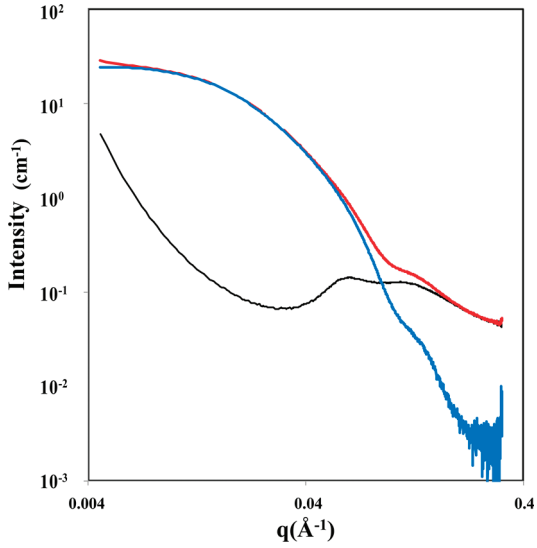

Figure 1. (Black) initial scattering of the solution before the addition of $NaBH_4$. (Red) final scattering after the growth of the nanorods where the signal of the micelles is still present. (Blue) final scattering of the nanoparticles after the subtraction of the initial diagram black leaving the scattering by the nanoparticles alone.

reports the scattering from the initial solution which contains micelles of CTAB and the final solution which contains still CTAB micelles and nanoparticles. To unravel the signal scattered by the nanoparticles, the background due to the signal micelles was systematically subtracted to all of the diagrams of the reactive solution along time. An example of such a subtraction for the final solution is shown in Figure 1.

As previously revealed by TEM,[26] the final suspension contains mainly nanorods together with a small fraction (10%) of spheres with a smaller volume than the one of nanorods. The scattering power of a given particles being proportional to the square of the volume, the total contribution of this population of spheres to the scattering was very low as compared to the one of cylinders. Accordingly it was neglected in the fitting procedure. The SAXS diagrams were fitted using the particular distribution of cylinders as revealed by the TEM.[26] Indeed, the distribution of width and length around their mean (R_0, L_0) is not decoupled as usually assumed.[22] Using an (L, R) representation of the cloud of nanoparticles, it was unraveled that the cloud is distributed along a line growing from an initial bifurcation point (BP) and with a slope θ. The fits were done using a summation of the intensities over this type of distribution:

$$I = N(\Delta\rho)^2 \iint f(u, v)V^2P_{cyl}(R_0, L_0, u, v)\,du\,dv \quad (1)$$

N being the number density of objects, $\Delta\rho$ is the scattering length density contrast between gold (at 11.5 keV) and water, $f(u,v)$ is the normalized distribution over u and v, and V and P_{cyl} are the volume and form factor of a cylinder of dimension L and R which are related to (u,v) and θ by

$$L = L_0 + u\cos(\theta) - v\sin(\theta)$$
$$R = R_0 + u\sin(\theta) + v\cos(\theta) \quad (2)$$

The distribution was taken Gaussian in u and v:

$$f(u, v) = \frac{1}{\sqrt{2\pi}\sigma_v \times \sqrt{2\pi}\sigma_u} e^{-v^2/2\sigma_v^2} \times e^{-u^2/2\sigma_u^2} \quad (3)$$

Two conditions are imposed on the distribution saying $L > 2 \times R$ and $R > R_{BP}$. Each kinetic was fitted backward starting from the longest time where the signal is the strongest.

TEM. The solutions contain at the end of the synthesis a large concentration of surfactants which have to be eliminated before TEM observation. To do so, the nanoparticles are separated by three cycles of centrifugation to extract the majority of them (9000 rpm during 1 h) and redispersed in pure water. The remaining supernatant was uncolored and translucent at the end of the procedure, indicating that all (or nearly) nanoparticles were extracted. Finally, one unique small drop of the surfactant free suspension of nanoparticles was deposited onto the TEM grid which was further dried in ambient air. The TEM measurements were performed using a 300 keV transmission electron microscope (TEM) Philips CM30. TEM micrographs were processed with a slow scan CCD camera.

RESULTS

In Situ SAXS: *R*(t) and *L*(t). The evolution along time of the scattering by the nanoparticles population is shown in Figure 2. The increase of the intensity at low q by several orders

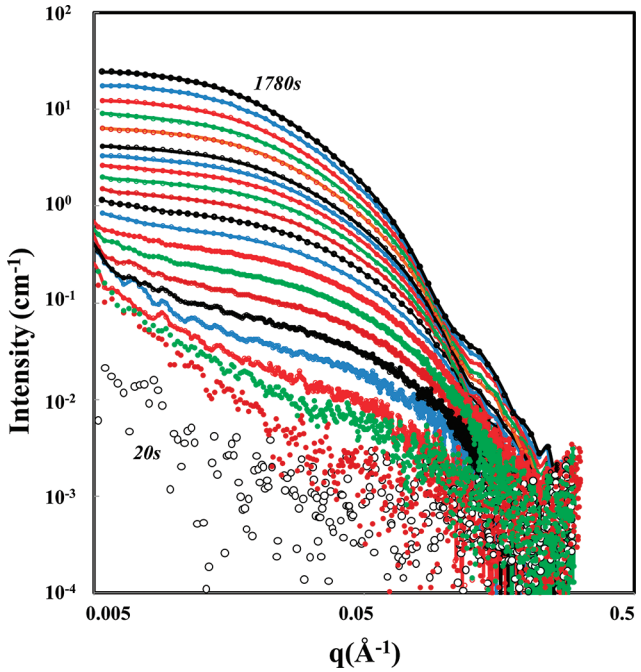

Figure 2. Time evolution from 20 s to 1780 s of the scattered intensity. The intensity reported at the absolute scale (cm^{-1}) and subtracted from the initial scattering diagram is totally due to the growing nanoparticles. The time resolution is 20 s but only some spectra are shown for clarity.

of magnitude revealed the nucleation and growth of nano-objects. The intensity was recorded every 20 s during 30 min to attain the saturation of the signal, ensuring that the diagram at 1780 s is the final one. The position in q of the transition from an almost constant intensity to a rapidly decreasing one at large

dx.doi.org/10.1021/cg2016116 | Cryst. Growth Des. 2012, 12, 1548–1555

q shifted to low q with the time of the reaction. This indicates the growth of at least one dimension of these nano-objects. Similarly, the damped oscillation in the Porod regime clearly present at large q is the signature of an increase of one dimension of these nano-objects (but not necessarily the same). To go deeper in the understanding of the scattering, a full fitting of the scattering with time was performed using eqs 1−3. The minimizations were operated at constant θ and σ_v to reduce the number of parameters, and hence L_0, R_0, and σ_u were used as minimizing parameters. A condition is to equal calculated and experimental Guinier regime (observed at low q), and the concentration of nanoparticles (in mol/L) was deduced by equaling the measure of the experimental invariant (between $q_{exp,min}$ and $q_{exp,max}$) with the theoretical one on the same q-range. The best fits are shown in Figure 3 and were obtained

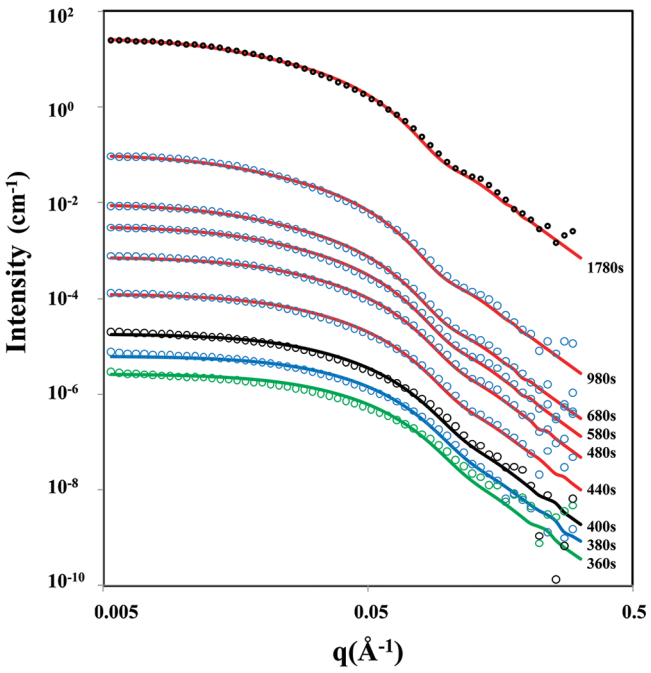

Figure 3. Experimental diagrams (circles) and calculated best fit (lines) are shown for some selected times. All the curves but the final one (1780 s) have been vertically shifted to enhance clarity and appreciation of the fit quality.

by using θ = 0.044 and σ_v = 0.68 nm. The final dimensions (L, R) of the nanorods are given in Table 1.

Table 1. Dimensions (R, L), Volume (V), and AR ($L/2R$) of the Nanorods with the Total Yields of the Reaction (Issued from SAXS) and the Total Concentration in Nanorods (Issued from SAXS Using Invariant Theorem) Are Given for Reference Synthesis and for Regrowth Experiments[a]

	R (nm)	L (nm)	V (nm^3)	$L/(2R)$	yield	concentration (mol/L)
initial growth	3.7	26.5	1127	3.6	0.45	2.44×10^{-8}
first regrowth (1)	4.1	36	1896	4.4	0.4	1.26×10^{-8}
second regrowth (2)	4.5	45	2856	5	0.4	0.85×10^{-8}

[a]First regrowth experiment (addition of the same volume of growth solution to initial growth solution for reference conditions). Second regrowth experiment (addition of a second volume of growth solution to the first overgrowth solution).

The evolution with time of the dimensions L, D and σ_u are shown in Figure 4. A first observation is that the particles are

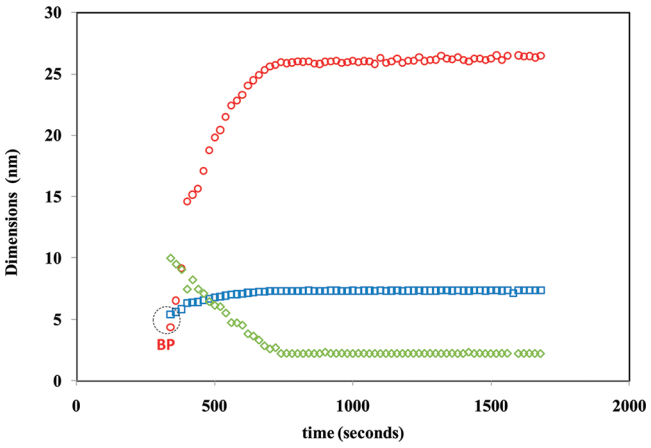

Figure 4. Time evolution of the nanorods dimensions obtained from the fitting of experimental data. The best fits (shown in Figure 3) are obtained using θ = 0.044 and σ_V = 0.68 nm (red circles) for length, (blue squares) for diameter, (green diamonds) for σ_u.

already at a size of 5.5 nm (L, D) after 300 s. This time corresponds to the nucleation period. Before 300 s the particles are very globular and no fitting was done. The second observation is that the length and width of the rods are increasing in parallel beyond this initial globular shape at the formerly called bifurcation point (BP).[26] The length growth rate is different (0.089 nm/s below 500 s) from the diameter growth rate (0.0074 nm/s below 500 s). During the growth period, the ratio of the two rates of growth is around 12 and the AR of the nanorods (as reported in Figure 5) increases with time from 1

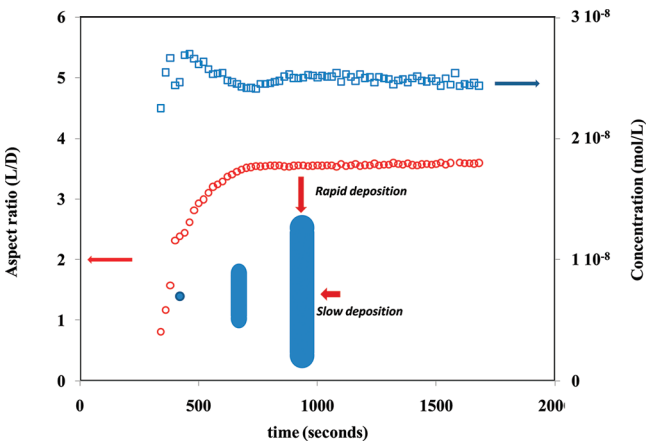

Figure 5. Time evolution of the AR (L/D) and concentration (mol/L) of the GNPs obtained from the best fits. A schematic drawing illustrates the geometrical result of two differential rates of growth between the basal and lateral faces.

at the BP to 3.6 at the end of the reaction. A striking point is that the concentration of nanoparticles is not increasing with time beyond the initial nucleation period. The formation of in situ seeds by the initial addition of borohydride is sufficiently rapid to induce a decoupling in time of the nucleation phase of these seeds and their growth into nanorods.

A major conclusion of these observations is that the anisotropy is acquired during the growth phase. We can even assume that if the growth was driven for longer time a higher

dx.doi.org/10.1021/cg2016116 | Cryst. Growth Des. 2012, 12, 1548−1555

anisotropic ratio would be obtained with nevertheless the final limit of 12.

Regrowth Experiments. To test this mechanism two successive regrowth experiments were performed. First, the same volume of a growth solution ($HAuCl_4$, CTABr, $AgNO_3$, and ascorbic acid but without borohydride salt) was added 24 h after to the final solution of a first synthesis (described in the experimental part). This step was repeated a second time for a second regrowth. The final scattering after regrowth 1 and 2 is shown in Figure 6 together with the first synthesis. The sizes

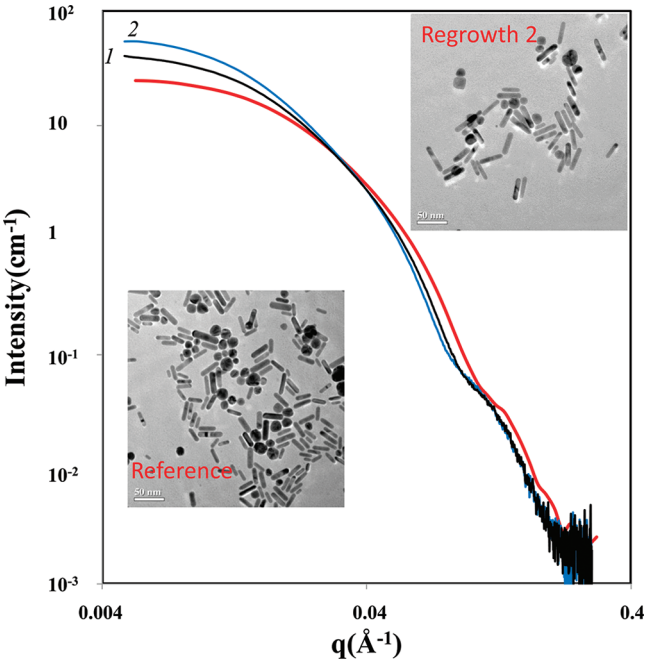

Figure 6. Regrowth experiment. In red, the final scattering diagram of the nanoparticles obtained following the reference synthesis. In black, the final scattering after a first regrowth experiment; in blue, the final scattering diagram after a second regrowth. Two TEM images are also shown for the reference conditions and the second regrowth. The longer particles present also a higher anisotropic ratio.

and concentrations of the nanorods deduced from the fits are reported in Table 1. One can note that (i) the concentration of nano-objects is diluted by 2 then by 3 as compared to the first synthesis. There is no extra nucleation when adding an extra volume of growth solution. (ii) The average volume of each particle is increased by a ratio 1.7 then 2.6 which are close to the ratio of added volume. The slight difference comes from a slight decrease of the yield of the reaction (0.4 instead of 0.45 for first one). Finally, the AR is also increasing from 3.6 to 4.4 then 5. The growth of the nanorods is even confirmed by the TEM images in Figure 6.

Yields (SAXS). The fitting procedure allows accessing the final concentration of nanoparticles and thus the yield of the reaction. However, the yield of the reaction could be measured by SAXS without any fitting procedure from the classical property of the invariant Q which depends only on the amount of the phases present in the solution:[28,29]

$$Q = 2\pi^2\phi(1-\phi)(\Delta\rho)^2 \qquad ([4])$$

$(\Delta\rho)$ is the scattering density length contrast between nanoparticles and solvent ($\Delta\rho = 1.08 \times 10^{12}$ cm^{-2} at 11.5 keV), Φ is the volume fraction of the scattering particles. The yield Y of the reaction can be deduced from the volume fraction Φ, using the density (d = 19.2 g/cm^3), the molar mass (M_w = 197) of gold, and the initial concentration of gold expressed in mol/cm^3:

$$Y = \frac{\phi d}{M_w}\frac{1}{C_{ini}} \qquad (5)$$

The time of the reaction can be estimated from eq 6 used to minimize the experimental data of the yield of the reaction versus time.

$$\%Au_{NP}(t) = 0.5 \times \left(1 + \tanh\left(\frac{t - t_i}{\Delta t}\right)\right) \times \%Au_{NP}(t_{final}) \qquad (6)$$

t_i is the abscise for the inflection point of the curve (at t_i, half of the gold has been transformed into nanoparticles) and Δt is the width of the tanh function (an estimation of the kinetic of the reaction, the higher Δt, the longer the kinetic).

Ascorbic Acid. Following the variations of the yield for different compositions in chemical compounds is very instructive to understand the effect of each component on the nanorods formation. As shown in Figure 7 and Figure S2, the final

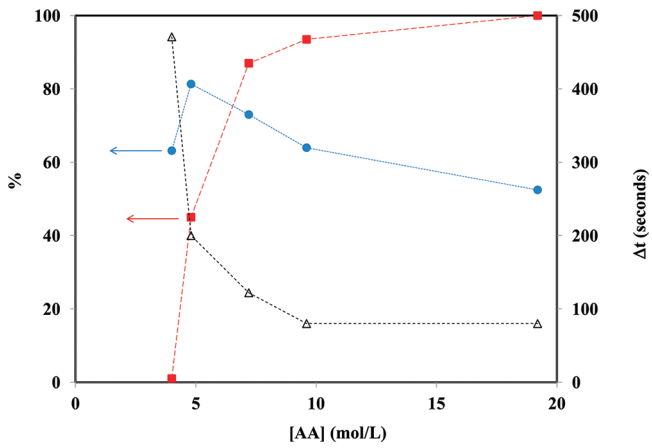

Figure 7. (Red squares): yield of the reaction, (blue circles): percentage of rods among the nanoparticles and (green diamonds): time of the reaction measured by Δt values, versus the ascorbic acid concentration. Lines are just a guide for the eyes.

yields of the reaction strongly depend on the ascorbic acid (AA) concentration. The reduction of Au(III) to Au(0) is a two step process with a stoichiometric ratio of 1.5 for a complete reaction (three electrons are necessary to reduce Au(III) into Au(0) while ascorbic acid gives two electrons). For an initial gold concentration of 3.5 mM, this implies a minimum concentration of ascorbic acid of 5.25 mM. Prior to the formation of seeds, ascorbic acid gives two electrons to reduce the 3.5 mM of Au(III) in Au(I). Without addition of seeds and thus the presence of a gold surface (either added from a tiny amount or formed in situ as in this work) ascorbic acid is not able to reduce Au(I) in Au(0). This is due to the presence of a large amount of CTABr. When seeds are formed by the borohydride addition, the remaining ascorbic acid amount reduces Au(I) into Au(0). For the reference conditions, only 1.3 mM of AA is left after the first step while 1.75 mM are required to reduce the 3.5 mM of Au(I) produced by the first step. Hence the theoretical yield should be 74% (also given by the eq 7 for

dx.doi.org/10.1021/cg2016116 | Cryst. Growth Des. 2012, 12, 1548–1555

understoichiometric conditions).

$$Y_{th} = \frac{([AA]_{ini} - [Au(III)]_{ini}) \times 2}{[Au(III)]_{ini}} \quad (7)$$

It is remarkable that the incomplete rate of conversion at 4.8 mM (45%) is even not stoichiometric. The same results are obtained for the overgrowth experiments operated in the same conditions with a final yield close to 40%. The difference between theoretical value and experimental one could be a pH effect since the ascorbate monoanion is the reducing species and the pH of the solution may be too low to operate a complete dissociation of the ascorbic acid. The effect of pH on the reaction rate in nanorods formation was already reported in the literature.[30,14] Recently, Bullen et al.[14] clearly identified that ascorbate monoanion is the primary reductant in the growth of GNRs and that the reaction rate is close to zero when the concentration of ascorbate monoanion is too low.

The final yield is therefore controlled by ascorbic acid concentration, 100% being attained for an excess AA concentration. However, in that case, the fraction of rods (obtained by TEM) among the different objects decreases markedly to reach only 50% when the yield is 100% (Figure 7). Said differently, the amount of gold under the shape of the nanorod is almost constant above C_{AA} = 4 mM, but there are more and more other types of nanoparticles. Accordingly, an extraction and purification by centrifugation would become trickier. An optimum concentration of AA is needed to optimize the total yield of the reaction but also the fraction of nanorods among the different shapes. Miranda et al.[31] had observed in their studies that an optimized ratio of AA (precisely the ascorbate monoanion) was necessary to increase the ratio of GNRs in the synthesis. They attributed this effect to the hydrotropic effect of ascorbic acid on the shape of the micelles even if the role of pH is certainly predominant. It is remarkable in our synthetic conditions that the increase of the polydispersity in shape with increasing the AA concentration is accompanied by a decrease of the time of reaction as shown in Figure 7. Anisotropic orientation seems to be correlated to an increase of the time of reaction.

$NaBH_4$ and $AgNO_3$. The optimization of rods to sphere ratio can also be obtained by changing the concentration of borohydride as already mentioned in our former article.[26] The borohydride salt has a strong influence on the initial induction time and the kinetic of reaction but not on the final yield as shown in Figure 8. It was formerly shown that a decrease in the borohydride concentration strongly modifies the ratio between rods and spheres with an optimum in the rods to spheres ratio[26] obtained at 1.25 μM. The role of the borohydride is thus to create in situ seeds for nanorods growth. The concentration of borohydride controls the size of the seeds, and the anisotropic growth is related to the position of the dimension of these seeds against the BP.[26] The optimization of rods can also be improved by the use of silver nitrate, since it is known to poison the reaction and promote anisotropy.[32,5,33,26] A moderation of the final yields of the reaction is imposed by the silver nitrate (Figure S3) together with saturation effect above 1 mM for the rod/sphere ratio.[26] For a given AA/$HAuCl_4$ molar ratio, an optimization of the synthesis can thus be obtained for a few seeds with a large amount of silver nitrate in the solution.

Yield (XANES). The yield of the reaction can also be obtained by XANES, but in that case one obtains the total fraction of Au(0) incorporated in the nanoparticles and residual (if any) free atoms or very small clusters in solution.

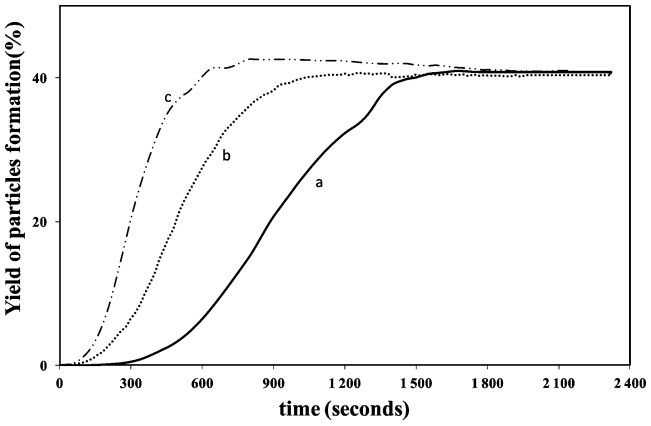

Figure 8. Influence of the concentration of borohydride on the yield of formation of nanoparticles (obtained by SAXS). The other concentrations correspond to the reference conditions when not mentioned (a) 0.625 μM $NaBH_4$, (b) 1.25 μM $NaBH_4$, (c) 15 μM $NaBH_4$.

The evolutions of the absorption spectra are presented in Figure 9. Before injection of ascorbic acid, the gold atoms are

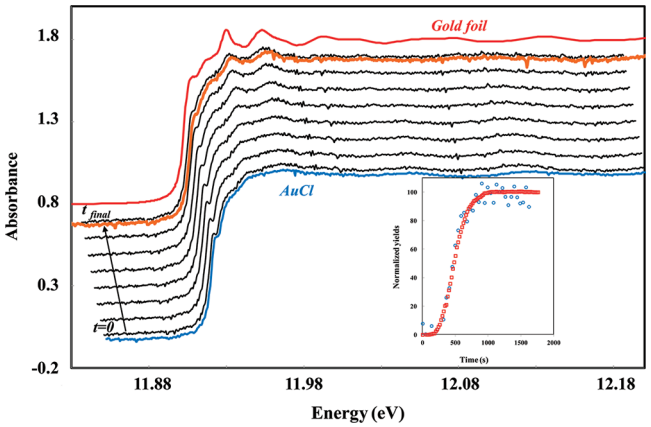

Figure 9. Time evolution of the aspect absorbance of the solution. Two references are shown: in blue the salt AuCl and in red the gold foil. The absorbance at t = 0 is perfectly reproduced by the AuCl signal meaning that all the ions are under the Au(I) state. The final state is also perfectly reproduced (brown line) by a linear combination of 60% Au(I) and 40% Au(0). Inset: yield of the total reduction of gold atoms as seen by XANES (blue circles) and of the nanoparticles formation as seen by SAXS (red squares); the yields have been normalized at their final values to highlight the kinetic behavior.

under the Au(III) oxidation state. Just after the addition of AA, the gold atoms are reduced to Au(I) as shown in Figure 9 where the first absorption spectra corresponds to Au(I). After the addition of borohydride, that defines the t = 0 of the kinetic, the absorption spectra $A(t)$ gradually includes features typical for the Au(0) state. Every absorption spectra $A(t)$ was indeed a linear combination from the two states Au(I) (A[Au(I)]) and Au(0) (A[Au(0)]: $A(t) = \alpha(t)\ A[Au(0)] + (1 - \alpha(t))\ A[Au(I)]$. The fraction $\alpha(t)$ represents the "total" fraction of gold atoms under the metallic state. This fraction leads to the monomer feeding rate of the reaction since Au(0) is the source of the nanoparticles whereas Au(III) ions were perfectly stable before the start of the reduction.

To improve the accuracy of $\alpha(t)$ with time, instead of performing a linear combination at each time, the absorbance

dx.doi.org/10.1021/cg2016116 | Cryst. Growth Des. 2012, 12, 1548–1555

$A_E(t)$ at a given energy was specifically followed with time for 25 selected energies, for which the variations were well marked (like the energies describing the two peaks of Au(0)): $\alpha(t)/\alpha_E(t) = A_E(t) - A_E(0)/A_E(t_f) - A_E(0)$. The treatment allows reaching a final accuracy of a few % (less than 2%) on the $\alpha(t)$ values. The normalized values of yield with time are plotted in the inset of Figure 9 together with the normalized yields of NPs value deduced from the SAXS. This allows concluding that the rate of variation of the yield in nanoparticles (from SAXS) and of the reduction of Au(I) in Au(0) (from XANES) is strictly identical. A strong conclusion is therefore that there are no Au(0) atoms free in solution (or even complexed within the micelles). This is in marked contrast with the case of a fast formation of gold nanospheres in toluene[24] where free Au(0) were indeed measured. Hence, the present result strongly supports that the reduction of Au(I) to Au(0) only occurs at the surface of the growing GNRs.

DISCUSSION

Using the absolute scaling of the scattered intensities, in situ SAXS experiments yield the concentration of particles with time together with their dimension. The concentration of nanoparticles with time as reported in the Figure 5 shows that beyond the initial nucleation, the number density of nanoparticles is constant during the growth phase. Nucleation and growth are thus separated for this seedless GNRs synthesis. This is the first demonstration that the growth of GNRs is occurring at constant number density which simplifies the discussion of the mechanism. Starting from a globular object around 5 nm, the anisotropy develops during the growth phase due to different rates of length and diameter.

The initial growth rate of length and diameter can be measured just at the end of the nucleation time, in the 340−460 s range. They are 0.089 nm/s for the length and 0.0074 nm/s for the diameter. With the present chemical conditions, the ratio is 12 and there is thus no hope (using this chemistry) to obtain nanorods with an AR beyond 12. The much lower final AR (3.6) comes from the final depletion of reactants during the first initial growth step. Accordingly, overgrowth experiments were used to obtain nanorods with higher AR and length. Overgrowth experiments have been described in the literature to optimize the length and/or the AR of the final nanorods,[16,35,34,36] but the obtained values have been scarcely related to the measured growth rate in the different directions. As shown in Table 1, two regrowth stages lead to an increase of the length and of the AR. The maximum AR should be obtained after several regrowth steps: the addition of a volume ratio of regrowth of 10 (100) will lead to an AR of 7.1 (9.5) for nanorods with average dimension 12.7 × 90 nm (24.8 × 236 respectively). It is important to note that the overgrowth is occurring with no secondary nucleation of new rods. This is due to the gradual dropwise addition of the growth solution into the final solution which maintains only a slight reincrease of gold salt in solution. Finally, the occurrence of a regrowth process discards a surfactant template effect in the nanorods formation. This observation is in agreement with the result from Chen et al.[35] for GNRs obtained without silver salt. After addition of different volumes of growth solution, they observed that the growth rate between longitudinal and transverse directions are constant for a large amount of added growth solution.

The experimental values for length and diameter rate are close to the ones reported in the literature for the seeded growth method at a much lower concentration (Table 2).

Table 2. Comparison with Literature

	present work from SAXS	ref 23 from SAXS	ref 23 from SAXS	ref 22 from SAXS	ref 17 from UV
$HAuCl_4$ (mM)	**3.5**	0.5	0.5	0.5	0.4
AA/Au	**1.37**	1.73	1.73	1.1	1.6
Ag/Au	**0.3**	0.04	0.16	0.08	0.15
length growth rate (nm/s)	**0.089**	0.18	0.08	0.047[a]	0.15
diameter growth rate (nm/s)	**0.0074**	0.04	0.01	0.012[a]	0.033
final AR	**3.6**	2	4	3.2	3.2

[a]Values directly extracted from the measurable time window.

In the three cases of the literature leading to GNRs with AR in the range 3−4, the measured rates obtained by SAXS are comparable to the one found in this work. This is not in agreement with the conclusion[14] that the reaction is of first order in Au(III) concentration since the concentration is multiplied by a factor 7. However, this stagnation of the growth rates certainly comes from the much higher Ag/Au used in the present work (poison effect of silver as described in the experimental section). The work using UV spectroscopic techniques[17] reports values in slight contrast with ref 23, for a comparable chemistry, and this shows the limits of comparison between different experimental techniques. However, the SAXS signal is a direct signature of the size dimension of nanoparticles.

The gold atom deposition is more efficient at the extremity than on the lateral sides of the GNRs. This has to be related to the different nature of the facets at the extremity or on the lateral sides of GNRs as recently described.[9,10] The nature of the poison at the surface of the facets strongly influences the rate of growth and thus the possible maximum anisotropic ratio. Moreover, comparing the different kinetic experiments, it can be observed that the development of anisotropy is also favored by a slow kinetic of reaction. As shown by Figure 7, an increase of the concentration of AA leads to a faster kinetic (smaller Δt) but at the cost of formation of isotropic nanoparticles (% of GNRs in the NP decreases). In that case, the obtained particles are bigger (data not shown), showing that there is no extra nucleation. Hence, the slower the reaction, the higher the yield in nanorods.[16] When the ratio of AA is increasing, the reducing activity of AA rises. Bullen et al.[14] have shown the important role of pH and AA/Au molar ratio to control the reactivity in such reaction. When the surface reduction is becoming faster, the source of the specific growth of certain facet is lost.

A central question regards the nature of the oxidation state of the gold reacting at the surface (both lateral and at the tip). It could be either the ion Au(I) implying a surface reduction plus an adsorption of the obtained Au(0) or directly a Au(0) adsorbing from a reservoir in the solution as already observed.[24] In the present work, the coupling between SAXS and XANES kinetics analysis yields an experimental demonstration of a surface reduction of Au(I) to Au(0) on the GNRs. No Au(0) monomer is found in the solution during the nanorods growth. It was shown that GNRs surface can catalyze the oxidation of ascorbic acid by dissolved oxygen[37] through the measurement of the electron injection and extraction during the redox reaction. This supports the catalysis role of the gold surface during the nanorods formation. Here, we have an experimental confirmation of the absence of a direct reduction in the solution of Au(I) to Au(0) during the growth process. The Au(I) must be adsorbed at

dx.doi.org/10.1021/cg2016116 | Cryst. Growth Des. 2012, 12, 1548−1555

the gold nanorods surface prior to its reduction by ascorbic acid (more precisely by the ascorbate monoanion). The diffusion of the Au(I) toward the gold surface, its surface reduction of Au(I), and the incorporation of Au(0) in the crystal are thus the limiting step of the process.

Finally, the surface reduction process also helps to understand why the GNRs present an almost constant section as seen in TEM. Any new surface defect created by the reduction-inclusion of a gold atom onto the surface of the particle will present a more reactive activity than the well formed 2D interfaces. Such a defect participates more efficiently to the catalysis by ascorbic acid of the freshly coming Au(I) complexes. Hence, defects of high energy cannot propagate perpendicular to the growing surfaces. Only the rates of alimentation in monomers at the surface contact are making the difference.

CONCLUSIONS

The use of a high concentration of $HAuCl_4$ (3.5 mM) combined with a higher $AgNO_3$ addition (Ag/Au = 0.3) allows producing GNRs with a controllable AR in the range 3.5−5 due to the final depletion of reactants. In principle, the AR could even be increased to 12, which is the ratio of length to diameter growth rates. Despite the use of an in situ production of seeds by direct tiny borohydride addition, the nucleation and growth are decoupled and the growth and overgrowth occur at a constant number of rods along a line defined by the ratio of the growth rates. From combined in situ SAXS and XANES, we also have demonstrated the growth of the gold nanorods is thus obtained by a surface reduction mechanism of the Au(I) at their surface.

ASSOCIATED CONTENT

Supporting Information

Figure S1: Comparison between the amount of Au(0) along time without and with an addition of borohydride. Figure S2: Influence of the concentration of ascorbic acid on the yield of the reaction with time. Figure S3: Influence of silver nitrate concentration on the yield of the reaction during the reaction. This information is available free of charge via the Internet at http://pubs.acs.org/.

AUTHOR INFORMATION

Corresponding Author

*E-mail: Olivier.Spalla@cea.fr.

ACKNOWLEDGMENTS

We want to thank M. Stucky and T. Narayanan from ID02 ESRF for useful discussions, Patrick Haltebourg for the mechanical design of sample environment, and P. E. Coulon from CEA/LSI for providing regular TEM access.

REFERENCES

(1) Murphy, C. J.; Thompson, L. B.; Alkilany, A. M.; Sisco, P. N.; Boulos, S. P.; Sivapalan, S. T.; Yang, J. A.; Chernak, D. J.; Huang, J. *J. Phys. Chem. Lett.* **2010**, *1*, 2867.
(2) Sharma, V.; Park, K.; Srinivasarao, M. *Mater. Sci. Eng. R* **2009**, *65*, 1.
(3) Pérez-Juste, J.; Pastoriza-Santos, I.; Liz-Marzán, L. M.; Mulvaney, P. *Coord. Chem. Rev.* **2005**, *249*, 1870.
(4) Jana, N. R.; Gearheart, L.; Murphy, C. J. *J. Phys. Chem. B.* **2001**, *105*, 4065.
(5) Nikoobakht, B.; El-Sayed, M. A. *Chem. Mater.* **2003**, *15*, 1957.
(6) Jana, N. R. *Small* **2005**, *1*, 875.
(7) Becker, R. *J. Col. Interface Sci.* **2010**, *343*, 25.
(8) Park, K.; Koerner, H.; Vaia, R. A. *Nano Lett.* **2010**, *10*, 1433.
(9) Carbo-Argibay, E.; Rodriguez-Gonzalez, B.; Gomez-Grana, S.; Guerrero-Martinez, A.; Pastoriza-Santos, I.; Perez-Juste, J.; Liz-Marzan, L. M. *Angew. Chem. Int. Ed* **2010**, *49*, 9397.
(10) Katz-Boon, H.; Rossouw, C.; Weyland, M.; Funston, A.; Mulvaney, P.; Etheridge, J. *Nano Lett.* **2011**, *11*, 273.
(11) Wang, Z. L.; Mohamed, M. B.; Link, S.; El-Sayed, M. A. *Surf. Sci.* **1999**, *440*, 809.
(12) Viswanath, B.; Kundu, P.; Halder, A.; Ravishankar, N. *J. Phys. Chem. C* **2009**, *113*, 16866.
(13) Perez-Juste, J.; Liz-Marzan, L.; Carnie, S.; Chan, D. Y. C.; Mulvaney, P. *Adv. Funct. Mater.* **2004**, *14*, 571.
(14) Bullen, C.; Zijlstra, P.; Bakker, E.; Gu, M.; Raston, C. *Cryst. Growth Des.* **2011**, *11*, 3375.
(15) Jana, N. R. *Angew. Chem.* **2004**, *43*, 1536.
(16) Sau, T. K.; Murphy, C. J. *Langmuir* **2004**, *20*, 6414.
(17) Gulati, A.; Liao, H.; Hafner, J. H. *J. Phys. Chem. B* **2006**, *110*, 22323.
(18) Boyes, E. D.; Gai, P. L. *Ultramicroscopy* **1997**, *67*, 219.
(19) Jana, N. R.; Gearheart, L.; Obare, S. O.; Murphy, C. J. *Langmuir* **2002**, *18*, 922.
(20) Takenaka, Y.; Kitahata, H. *Phys. Rev. E* **2009**, *80*, 020601.
(21) Xiang, Y.; Wu, X.; Liu, D.; Feng, L.; Zhang, K.; Chu, W.; Zhou, W.; Xie, S. *J. Phys. Chem. C* **2009**, *112*, 3203.
(22) Henkel, A.; Schubert, O.; Plech, A.; Sönnichsen, C. *J. Phys. Chem. C* **2009**, *113*, 10390.
(23) Morita, T.; Tanaka, E.; Inagaki, Y.; Hotta, H.; Shingai, R.; Hatakeyama, Y.; Nishikawa, K.; Murai, H.; Nakano, H.; Hino, K. *J. Phys. Chem. C* **2010**, *114*, 3804.
(24) Abécassis, B.; Testard, F.; Kong, Q.; Baudelet, F.; Spalla, O. *Langmuir* **2010**, *26*, 13847.
(25) Harada, M.; Einaga, H. *Langmuir* **2007**, *23*, 6536.
(26) Hubert, F.; Testard, F.; Rizza, G.; Spalla, O. *Langmuir* **2010**, *26*, 6887.
(27) Zijlstra, P.; Bullen, C.; Chon, J.; Gu, M. *J. Phys. Chem. B* **2006**, *110*, 19315.
(28) Porod, G. *Small Angle Scattering of X-rays*; Academic Press: New York, 1982; Chapter General Theory.
(29) Abécassis, B.; Testard, F.; Spalla, O.; P., B. *Nano Lett.* **2007**, *7*, 1723.
(30) Busbee, B. D.; Obare, S. O.; Murphy, C. J. *Adv. Mater.* **2003**, *15*, 414.
(31) Miranda, O. R.; Dollahon, N. R.; Ahmadi, T. S. *Cryst. Growth Des.* **2006**, *6*, 2747.
(32) Liu, M.; Guyot-Sionnest, P. *J. Phys. Chem. B* **2005**, *109*, 22192.
(33) Jana, N. R.; Gearheart, L.; Murphy, C. J. *Adv. Mater.* **2001**, *13*, 1389.
(34) Keul, H. A.; Möller, M.; Bockstaller, M. R. *Langmuir* **2007**, *23*, 10307.
(35) Chen, H. A.; Liu, R. S.; Asakura, K.; Jang, L. Y.; Leee, J. F. *J. Phys Chem. C* **2007**, *111*, 18550.
(36) Song, J. H.; Kim, F.; Kim, D.; Yang, P. *Chem.—Eur. J.* **2005**, *11*, 910.
(37) Novo, C.; Funston, A. M.; Mulvaney, P. *Nat. Nanotechnol.* **2008**, *3*, 598.